

Article

Structure and Bonding in $\text{CsNa}_2\text{Hg}_{18}$, a New Ternary Amalgam with Strong Coulombic Bonding Contributions

Timotheus Hohl ¹, Frank Tambornino ²  and Constantin Hoch ^{1,*}¹ Department Chemie, LMU München, Butenandtstraße 5-13(D), D-81377 München, Germany² Fachbereich Chemie, Universität Marburg, Hans-Meerwein-Straße 4, D-35043 Marburg, Germany

* Correspondence: constantin.hoch@cup.uni-muenchen.de; Tel.: +49-89-2180-77421

Abstract: The new ternary amalgam $\text{CsNa}_2\text{Hg}_{18}$ was synthesised from the elements in an unconventional low-temperature procedure. It crystallises in a tetragonal structure type (space group $I4/mmm$, $a = 7.3054(7)$ and $c = 20.046$ Å) and combines ionic and metallic bonding contributions. In the crystal structure, Cs and Na atoms are embedded in a Hg scaffold with highly covalent Hg–Hg bonding. The alkali metal atoms are coordinated exclusively by Hg atoms in unusual environments with coordination numbers CN = 24 for Cs and CN = 16 for Na. Polar amalgams are suitable model systems for studying the parameters influencing the ‘bad metal behaviour’ in polar intermetallic phases. We present structural studies on the basis of powder and single crystal diffraction data together with measurements of the specific resistivity and DFT calculations of the electronic structure. For $\text{CsNa}_2\text{Hg}_{18}$, a high specific resistivity can be observed, but the Ioffe–Regel saturation of the resistivity is expressed much less than in other polar amalgams.

Keywords: ternary amalgams; alkali metal amalgams; crystal structure; polar metallic bonding; band structure; specific resistivity



Citation: Hohl, T.; Tambornino, F.; Hoch, C. Structure and Bonding in $\text{CsNa}_2\text{Hg}_{18}$, a New Ternary Amalgam with Strong Coulombic Bonding Contributions. *Crystals* **2022**, *12*, 1679. <https://doi.org/10.3390/cryst12111679>

Academic Editor: Jianying Huang

Received: 27 October 2022

Accepted: 12 November 2022

Published: 21 November 2022

Publisher’s Note: MDPI stays neutral with regard to jurisdictional claims in published maps and institutional affiliations.



Copyright: © 2022 by the authors. Licensee MDPI, Basel, Switzerland. This article is an open access article distributed under the terms and conditions of the Creative Commons Attribution (CC BY) license (<https://creativecommons.org/licenses/by/4.0/>).

1. Introduction

The number of preparative and structural studies on binary amalgams of less noble metals is considerable [1,2]. Their structural chemistry is extremely rich, owing to the versatile bonding characteristics of negatively polarised $\text{Hg}^{\delta-}$. As Hg has a thermodynamically unfavourable electron affinity and does not form an anion in the gas phase [3], a Zintl-analogous anion Hg^- is unknown, yet a certain negative partial charge can be stabilised in the crystal lattice. This partial charge increases with the Hg content of the amalgams as the unfavourable electron density can be better delocalised over a larger number of Hg atoms. A hypothetical Hg^- would have the electron configuration $[\text{Xe}]4f^{14}5d^{10}6s^26p^1$, and for this reason, p – p σ interaction would be expected. Mixing of s and p (and d) states is, to a certain extent, hampered by spin-orbit coupling and relativistic effects, which make the structural chemistry of amalgams so unique. A versatile mixture of metallic, ionic, and covalent bonding contributions occurs, depending on the amount of Hg present in the amalgams, on the quotients of the atomic radii, and on the extent of the electron transfer from the electropositive metal to mercury. In Hg-poor amalgams, isolated Hg atoms occur, but with rising Hg content, soon Hg–Hg bonding is found. In some amalgams, square $[\text{Hg}_4]$ groups are present with 90° interatomic angles, corroborating the abovementioned p – p σ bonding situation [4–6]. Further, $[\text{Hg}_8]$ cubes or ladders of $[\text{Hg}_4]$ squares are known [7,8]. In Hg-rich amalgams, more and more d participation leads to complex networks, and the $[\text{Hg}_{12}]$ icosahedron is one of the predominant structural motifs. In this case, the close relation of $\text{Hg}^{\delta-}$ to the electron-deficient p^1 metals and their structures becomes evident.

A second frequent structural feature contrasting the covalent Hg–Hg interactions is the tendency of the polar amalgams to form coordinated polyhedra of Hg atoms (‘anions’) around the less noble metal atoms (‘cations’). This, of course, is more pronounced

in Hg-rich amalgams for reasons of stoichiometry, but also in Hg-poor amalgams, the tendency to avoid cation–cation contacts becomes evident. Hg-coordinated polyhedra around the electropositive metal atoms vary depending on the atomic sizes, from [MHg₈] (e.g., in HgMn [9] with $r_{Mn}/r_{Hg} = 0.9$) to [MHg₂₄] (e.g., in the title compound CsNa₂Hg₁₈ with $r_{Cs}/r_{Hg} = 1.7$). As Hg is a medium to small-sized metal atom ($r_{Hg}^{met} = 150$ pm) [10], an atomic radii quotient r_M/r_{Hg} of roughly 1 is a common case. Therefore, in Hg-rich amalgams, coordination numbers CN of ≥ 12 occur frequently, and (anti-)cuboctahedra [MHg₁₂], icosahedra [MHg₁₂], and Frank–Kasper polyhedra [MHg_{14–16}] are common structural motifs.

The third structural motif often found in amalgams of less noble metals is the tendency to form closest sphere packings or structural cut-outs thereof. The large structure family of amalgams of Ag₁₄Gd₅₄-related structures very clearly shows the tendency towards the formation of an hcp lattice [11,12]. The structures of other amalgams can be rationalised as arrangements of more or less close-packed nets; others show arrangements of octahedra and tetrahedra as motifs from closest sphere packings. In all of these cases, the metal atomic radius quotient is close to 1.

The three structural motifs—covalent Hg networks, coordination polyhedra [MHg_n], and variations of closest sphere packings—often occur at the same time, and it is, to a certain extent, arbitrary which aspect is emphasised in the respective structural descriptions. A structural discussion focussing on ionic polarity and electron transfer from the less noble metal on Hg may utilise the more ‘ionic picture’ of coordination polyhedra, while a more ‘intermetallic picture’ may focus on the sphere packing aspects. Emphasising the electronic configuration of the Hg atoms may afford the ‘covalent picture’, highlighting the Hg network with Hg–Hg bonding. In many cases, all three aspects can be illustrated for a given amalgam structure.

In contrast to the manifold studies on binary amalgams, knowledge of ternary amalgams is scarce. The only examples of ternary amalgams containing two different less noble metals are NaK₂₉Hg₄₈ [13], Li₂MgHg [14], Li₆Ca₁₇Hg₉, Li₆Sr₁₇Hg₉, and Li₆Yb₁₇Hg₉ [15]. A larger number of ternary amalgams with the participation of transition metals together with less noble metals also are known. All structurally characterised ternary amalgams with the participation of at least one less noble metal are compiled in Table 1.

Ternary amalgams are only reported in the Hg-poor region $M:Hg \leq 1:2.5$. The Hg-richest phases have the composition A_3BHg_{10} . For the abovementioned reasons, we attempt, for the first time, a systematic study on ternary Hg-rich amalgams of less noble metals. As Hg shows high reactivity towards a large number of metallic elements, the outcome of a study designated to ternary amalgams can be expected to be rich. CsNa₂Hg₁₈ is an example of a ternary amalgam with high ionic bonding contributions, and it adopts a new structure type with an unprecedented Hg network.

Table 1. Ternary amalgams described in the literature containing at least one less noble (=alkali, alkaline earth, or lanthanoid) metal. Data are compiled from Pearson’s Crystal Data [16].

Phase	Space Group	Structure Type	Lit.	Phase	Space Group	Structure Type	Lit.
Ternary amalgams with alkali metals							
Li ₂ MgHg	<i>Fm</i> $\bar{3}$ <i>m</i>	Cu ₂ MnAl	[14]	KAsHg	<i>P</i> 6 ₃ / <i>mmc</i>	BeZrSi	[17]
Li ₂ GeHg	<i>Fm</i> $\bar{3}$ <i>m</i>	Cu ₂ MnAl	[18]	KSbHg	<i>P</i> 6 ₃ / <i>mmc</i>	BeZrSi	[17]
Li ₆ Ca ₁₇ Hg ₉	<i>Im</i> $\bar{3}$ <i>m</i>	own	[15]	KC ₄ Hg	<i>Fddd</i>	own	[19]
Li ₆ Sr ₁₇ Hg ₉	<i>Im</i> $\bar{3}$ <i>m</i>	Li ₆ Ca ₁₇ Hg ₉	[15]	K ₄ Ge _{21.3} Hg _{1.7}	<i>Pm</i> $\bar{3}$ <i>n</i>	Na ₄ Si ₂₃	[20]
Li ₆ Yb ₁₇ Hg ₉	<i>Im</i> $\bar{3}$ <i>m</i>	Li ₆ Ca ₁₇ Hg ₉	[15]	K ₄ Ge _{21.4} Hg _{1.6}	<i>Pm</i> $\bar{3}$ <i>n</i>	Na ₄ Si ₂₃	[20]
LiTl _{0.5} Hg _{0.5}	<i>Pm</i> $\bar{3}$ <i>m</i>	CsCl	[21]	K ₄ Sn ₂₁ Hg ₂	<i>Pm</i> $\bar{3}$ <i>n</i>	Na ₄ Si ₂₃	[22]
Na ₂ SnHg	<i>F</i> $\bar{4}$ <i>3m</i>	Li ₂ AgSb	[23]	K ₈ In ₁₀ Hg	<i>P</i> 6 ₃ / <i>m</i>	own	[24]
Na ₂ PbHg	<i>F</i> $\bar{4}$ <i>3m</i>	Li ₂ AgSb	[23]	Rb ₄ Ge _{21.3} Hg _{1.7}	<i>Pm</i> $\bar{3}$ <i>n</i>	Na ₄ Si ₂₃	[20]
Na ₅ Sn _{9.6} Hg _{2.4}	<i>Pbcn</i>	own	[25]	Rb ₄ Ge _{21.5} Hg _{1.5}	<i>Pm</i> $\bar{3}$ <i>n</i>	Na ₄ Si ₂₃	[20]
NaTl _{0.5} Hg _{0.5}	<i>Fd</i> $\bar{3}$ <i>m</i>	NaTl	[26]	Rb ₄ Sn ₂₁ Hg ₂	<i>Pm</i> $\bar{3}$ <i>n</i>	Na ₄ Si ₂₃	[22]

Table 1. Cont.

Phase	Space Group	Structure Type	Lit.	Phase	Space Group	Structure Type	Lit.
Na _{2.1} C ₆₀ Hg _{0.2}	<i>Pa</i> $\bar{3}$	own	[27]	Cs ₄ Sn ₂₁ Hg ₂	<i>Pm</i> $\bar{3}n$	Na ₄ Si ₂₃	[22]
Na ₂ C ₆₀ Hg _{0.2}	<i>Pa</i> $\bar{3}$	Na ₂ RbC ₆₀	[27]				
NaK ₂₉ Hg ₄₈	<i>Pm</i> $\bar{3}n$	own	[13]				
Ternary amalgams with alkaline earth metals							
MgLi ₂ Hg	<i>Fm</i> $\bar{3}m$	Cu ₂ MnAl	[14]	BaGa _{0.8} Hg _{5.2}	<i>Cmcm</i>	own	[28]
Mg ₂₁ Ga ₅ Hg ₃	<i>I4</i> ₁ / <i>a</i>	Pt ₈ Al ₂₁	[29]	BaGa _{1.9} Hg _{2.1}	<i>I4</i> ₁ / <i>amd</i>	own	[28]
Mg ₂ Au _{0.5} Hg _{0.5}	<i>Pnma</i>	Co ₂ Si	[30]	Ba ₃ Ga _{0.2} Hg _{10.8}	<i>Pmmn</i>	Ba ₃ ZnHg ₁₀	[28]
MgAu _{0.67} Hg _{0.33}	<i>Pm</i> $\bar{3}m$	CsCl	[30]	BaIn _{1.1} Hg _{0.9}	<i>Imma</i>	KHg ₂	[31]
Mg ₃ Au _{0.7} Hg _{0.3}	<i>P6</i> ₃ / <i>mmc</i>	Na ₃ As	[30]	BaIn _{1.7} Hg _{2.3}	<i>I4</i> / <i>mmm</i>	BaAl ₄	[28]
Ca ₁₇ Li ₆ Hg ₉	<i>Im</i> $\bar{3}m$	own	[15]	BaIn _{2.8} Hg _{8.2}	<i>Pm</i> $\bar{3}m$	BaHg ₁₁	[32]
CaSn _{0.7} Hg _{1.3}	<i>P6</i> / <i>mmm</i>	UHg ₂	[33]	BaIn _{1.2} Hg _{4.8}	<i>Pnma</i>	BaHg ₆	[34]
CaSnHg	<i>P6</i> ₃ / <i>mc</i>	LiGaGe	[33]	BaIn _{3.1} Hg _{3.9}	<i>Cmmm</i>	own	[32]
CaPbHg	<i>P6</i> ₃ / <i>mmc</i>	BeZrSi	[33]	Ba ₃ InHg ₁₀	<i>Immm</i>	La ₃ Al ₁₁	[28]
Ca ₄ Zn _{4.5} Hg _{4.5}	<i>P4</i> ₃ <i>m</i>	Cu ₉ Al ₄	[35]	BaTl ₂ Hg ₂	<i>P4</i> ₂ / <i>mnm</i>	own	[36]
Ca ₄ Cu _{4.5} Hg _{4.5}	<i>P4</i> ₃ <i>m</i>	Cu ₉ Al ₄	[35]	BaTl _{3.2} Hg _{0.8}	<i>C2</i> ₁ / <i>m</i>	EuIn ₄	[37]
Ca ₄ Au _{4.5} Hg _{4.5}	<i>P4</i> ₃ <i>m</i>	Cu ₉ Al ₄	[35]	Ba ₄ Ge ₁₉ Hg ₄	<i>Pm</i> $\bar{3}n$	Na ₄ Si ₂₃	[38]
SrSnHg	<i>P6</i> ₃ / <i>mc</i>	LiGaGe	[33]	BaSnHg	<i>P6</i> ₃ / <i>mmc</i>	BeZrSi	[33]
SrPbHg	<i>P6</i> ₃ / <i>mc</i>	LiGaGe	[33]	BaPbHg	<i>Imma</i>	KHg ₂	[33]
SrTl ₂ Hg ₂	<i>P4</i> ₂ / <i>mnm</i>	BaTl ₂ Hg ₂	[36]	Ba ₃ ZnHg ₁₀	<i>Pmmn</i>	own	[39]
Sr ₁₇ Li ₆ Hg ₉	<i>Im</i> $\bar{3}m$	Ca ₁₇ Li ₆ Hg ₉	[15]	BaZn _{0.6} Hg _{3.4}	<i>I4</i> ₃ <i>d</i>	own	[39]
Sr ₃ In _{10.3} Hg _{0.7}	<i>Immm</i>	La ₃ Al ₁₁	[40]	Ba ₂₀ Zn ₅ Hg ₉	<i>F4</i> ₃ <i>m</i>	own	[41]
SrIn _{3.4} Hg _{0.6}	<i>C2</i> / <i>m</i>	EuIn ₄	[40]	Ba ₃ CdHg ₁₀	<i>Immm</i>	La ₃ Al ₁₁	[28]
SrIn _{1.3} Hg _{2.7}	<i>C2</i> / <i>m</i>	EuIn ₄	[40]	Ba ₂₀ Cd ₄ Hg ₉	<i>F4</i> ₃ <i>m</i>	own	[41]
SrIn _{0.9} Hg _{3.0}	<i>C2</i> / <i>m</i>	EuIn ₄	[40]				
SrIn _{1.3} Hg _{1.8}	<i>C2</i> / <i>m</i>	SrIn _{1.2} Hg _{1.3}	[40]				
SrIn _{3.0} Hg _{1.0}	<i>I4</i> / <i>mmm</i>	CeAl ₂ Ga ₂	[40]				
SrIn _{2.8} Hg _{1.2}	<i>I4</i> / <i>mmm</i>	CeAl ₂ Ga ₂	[40]				
SrIn ₂ Hg ₂	<i>I4</i> / <i>mmm</i>	CeAl ₂ Ga ₂	[40]				
Ternary amalgams with lanthanoid metals							
CePdHg	<i>P6</i> ₂ <i>m</i>	ZrNiAl	[42]	EuSnHg	<i>P6</i> ₃ / <i>mc</i>	LiGaGe	[33]
PrPdHg	<i>P6</i> ₂ <i>m</i>	ZrNiAl	[42]	EuPbHg	<i>P6</i> ₃ / <i>mc</i>	LiGaGe	[33]
Pr ₆ Fe ₁₃ Hg	<i>I4</i> / <i>mcm</i>	Pr ₆ Fe ₁₃ Ge	[43]	GdPdHg	<i>P6</i> ₂ <i>m</i>	ZrNiAl	[42]
Nd ₆ Fe ₁₃ Hg	<i>I4</i> / <i>mcm</i>	Pr ₆ Fe ₁₃ Ge	[43]	YbSnHg	<i>P6</i> ₃ / <i>mc</i>	LiGaGe	[33]
SmPdHg	<i>P6</i> ₂ <i>m</i>	ZrNiAl	[42]	YbPbHg	<i>P6</i> ₃ / <i>mmc</i>	BeZrSi	[33]
				Yb ₁₇ Li ₆ Hg ₉	<i>Im</i> $\bar{3}m$	Li ₆ Ca ₁₇ Hg ₉	[15]

2. Results and Discussion

2.1. Crystal Structure of CsNa₂Hg₁₈

The first single crystals of CsNa₂Hg₁₈ were observed in a sample with a weighed ratio of Cs:Na = 1:1 and a large Hg surplus. The new amalgam was found with Cs₃Hg₂₀ as the only impurity. An optimised synthesis yielded phase-pure material; details are given in Section 3.1.

CsNa₂Hg₁₈ crystallises in a new structure type with tetragonal symmetry in space group *I4*/*mmm*. Its crystal structure is built from one Cs, one Na, and three crystallographically independent Hg positions. For basic crystallographic data and for details on data collection and handling, see Table 2. The structure of this new Hg-rich amalgam can be described by several different concepts, which is a common finding for Hg-rich amalgams [11,44,45] and reflects the interplay of metallic and ionic bonding on the structural level.

Table 2. Crystallographic data and details on single crystal data collection, structure solution, and refinement for CsNa₂Hg₁₈. Data collection was performed at room temperature. All standard deviations are given in parentheses in the units of the last digit.

Composition	CsNa ₂ Hg ₁₈
Crystal system	tetragonal
Space group	<i>I4</i> / <i>mmm</i> , No. 139

Table 2. Cont.

Lattice parameters <i>a</i> , <i>c</i> (Å)	7.3054(7), 20.046(3)
<i>V</i> (Å ³)	1069.8(3)
<i>Z</i>	2
Density (X-ray) (g·cm ⁻³)	11.76
Diffractometer	STOE IPDS 1
Absorption coeff. μ (mm ⁻¹)	Ag-K α radiation, $\lambda = 0.56086$ Å 71.24
θ range (°)	2.34–26.24
Index range	$-9 \leq h, k \leq 9,$ $-27 \leq l \leq 27$
No. of collected refl.	5786
No. of independent refl.	448
No. of indep. refl. ($I \geq 2\sigma(I)$)	363
R_{int}	0.1694
R_{σ}	0.0571
$F(000)$	3034
Corrections	Lorentz, polarisation, absorption effects
Absorption correction	numerical, indexed crystal faces [46,47]
Structure solution	direct methods [48]
Structure refinement	full-matrix least-squares on F^2 [48]
No. of L.S. parameters	21
GooF	1.015
R values ($I \geq 2\sigma(I)$)	$R1 = 0.0325, wR2 = 0.0649$
R values (all data)	$R1 = 0.0453, wR2 = 0.0679$
Res. $\rho(e^-)$ min/max ($e^- \text{Å}^{-3}$)	−3.108/+2.331
Extinction coefficient	0.0029(2)
CCDC deposition No.	2031829

A more ionic structural picture results from the description of the crystal structure using coordination polyhedra of the ‘anionic’ Hg atoms around the ‘cations’ Cs1 and Na1 (for fractional atomic coordinates, site symmetries, and isotropic thermal displacement parameters, see Table 3, anisotropic displacement parameters are compiled in Table 4). This representation of the crystal structure of CsNa₂Hg₁₈ is shown in Figure 1, centre and right. The next neighbouring atoms of both Cs1 and Na1 are only Hg atoms with a clear separation of the interatomic distances (see Table 5) from the next shell of atoms. For the large atom Cs1, a 24-vertex polyhedron [CsHg₂₄] with site symmetry $4/m\bar{m}m$ is found. It is a rhombicuboctahedron consisting of 18 square and 8 triangular faces. The point symmetry of the ideal Archimedean polyhedron would be $m\bar{3}m$. However, the tetragonal distortion in this crystal structure is quite small, see Figure 1, top right. All Hg–Hg distances range between 2.844(1) and 3.062(1) Å and are well in the range of Hg–Hg distances observed in other Hg-rich amalgams. The Cs–Hg interatomic distances are rather large in comparison with those found for other Cs amalgams (see Figure 2), which can be attributed to the unusually large coordination number. The coordination number of 24 and the rhombicuboctahedron as a coordination polyhedron are quite rare in structural chemistry. Pearson’s Crystal Database [16] lists 2299 entries for crystal structures in which at least one atomic site has CN = 24. The largest number corresponds to structures with partially occupied atomic positions, such as CaF₂- or α -AgI-related structures, where unreasonably short distances between atoms occur. In structures with fully occupied [AB₂₄] coordination spheres, two major groups can be distinguished: 468 of them belonging to the group of clathrates Type I containing truncated hexagonal trapezohedra [NaSi₂₄], and 125 entries are phases crystallising in the NaZn₁₃ structure type where the Na position atoms are coordinated in snub cubes [NaZn₂₄]. These two polyhedra are shown in Figure 3 and are the most prominent for atoms having coordination number 24. The rhombicuboctahedron has (to our knowledge) not been observed yet. However, rotation of the square faces of a snub cube by 28.7° results

in a rhombicuboctahedron, and an intermediate polyhedron with a rotation of only 8.7° was already found in CsIn_{12} [49]. The $[\text{NaHg}_{16}]$ coordination polyhedron shown in Figure 1 on the lower right can be described as a snub square antiprism (Johnson solid No. J_{85}). Its ideal point symmetry (D_{4d}) is reduced to $C_{4v} = 4mm$. The Hg–Hg distances in this polyhedron are well within the range of commonly observed interatomic distances within Hg-rich amalgams. The Na–Hg interatomic distances are well in agreement with those found in other Na amalgams, see Figure 2. Here again, the coordination polyhedron is an uncommon one: for coordination number 16 (8644 entries in *Pearson's Crystal Database*), there are several polyhedra, see Figure 3. By far the most frequent one, with 7005 entries, is the 16-vertex Frank–Kasper polyhedron (fourcapped truncated tetrahedron), which occurs, e.g., in the MgCu_2 -type structures, followed by a fourcapped hexagonal prism occurring in AlB_2 -related structures. The snub square antiprism observed here seems to be a rather exotic solution for the realisation of coordination number 16, see Figure 3. The cation topology can be described in a packing with a defect- ThCr_2Si_2 topology in the sense of $\text{Th}\square_2\text{Si}_2$.

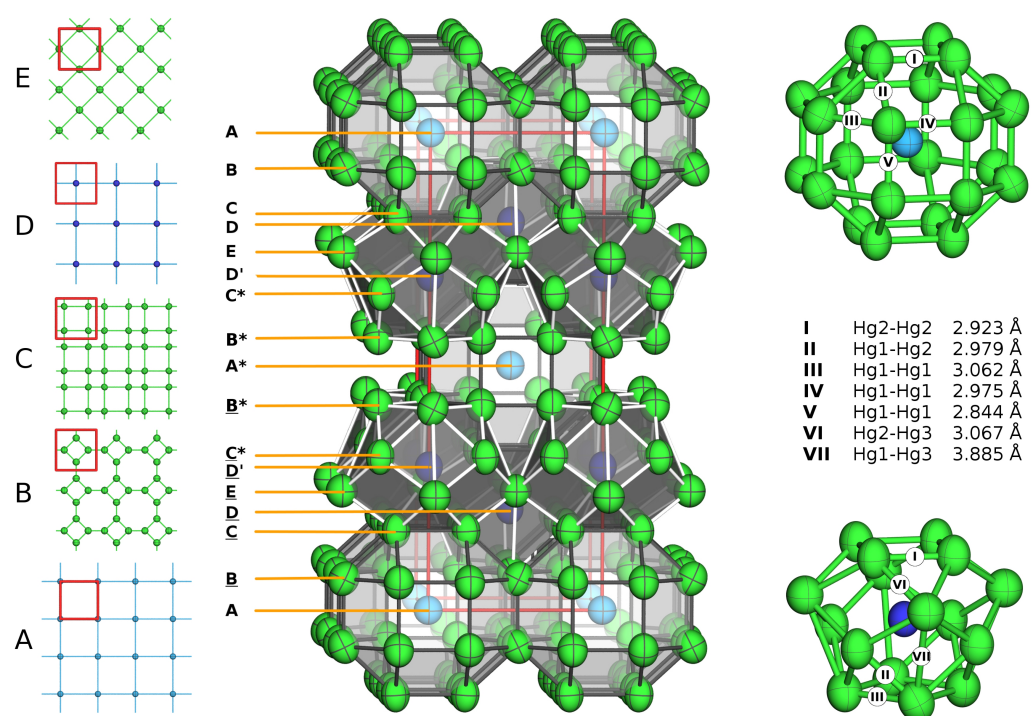


Figure 1. Crystal structure of $\text{CsNa}_2\text{Hg}_{18}$. Center: unit cell with polyhedra representation for Cs1 and Na1. Hg: green, Cs: light blue, Na: dark blue. Polyhedra around Cs1 are drawn in light grey, and polyhedra around Na1 in dark grey. The crystallographic c -axis points upwards; the unit cell is marked in red. For all atoms, ellipsoids are shown on a 99% probability level. Left: Net representation with net A (Cs atoms) at $z = 0$, net B (Hg1 atoms) at $z \approx 0.07$, net C (Hg2 atoms) at $z \approx 0.17$, net D (Na atoms) at $z \approx 0.20$ and net E (Hg3 atoms) at $z = 1/4$. The stacking sequence marked next to the unit cell is coded with nets X and X' being related by rotation around the c axis by 45° , X and X* related by the body centring and X and \bar{X} related by the horizontal mirror plane at height $z = 1/2$. Right: coordination polyhedra around Cs1 (top) and around Na1 (below).

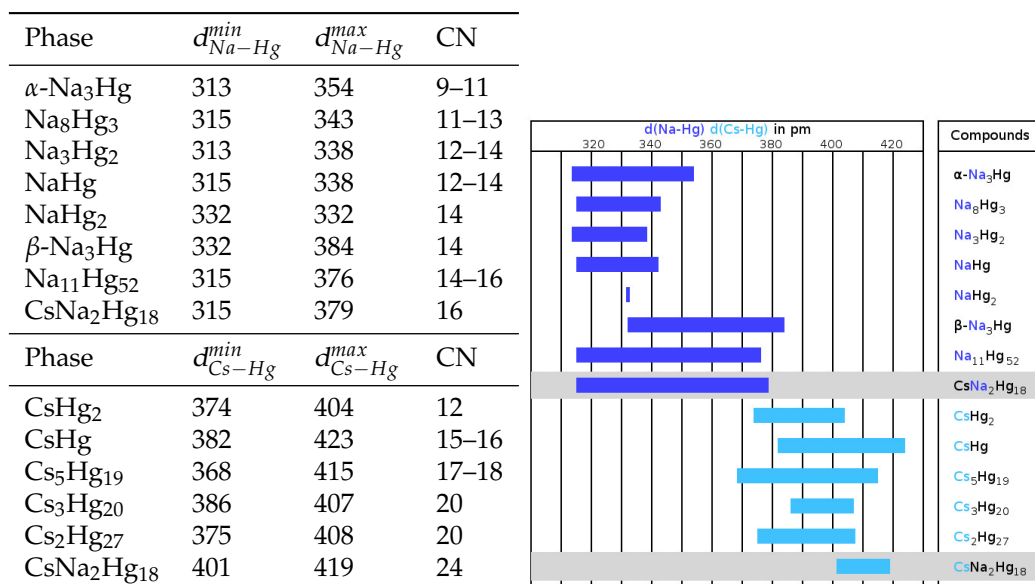


Figure 2. Na–Hg and Cs–Hg interatomic distances (in pm) and coordination numbers vs. Hg in CsNa₂Hg₁₈ in comparison to those found in the literature [5,6,8,11,50–55] for binary Na and Cs amalgams, respectively.

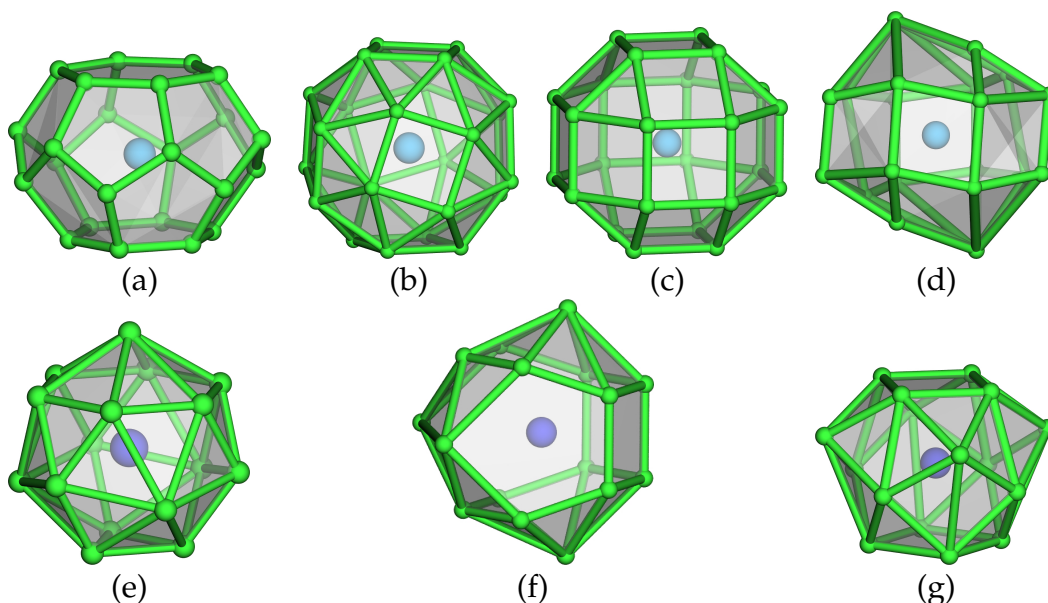


Figure 3. Upper row: polyhedra for coordination number 24: (a) truncated hexagonal trapezohedron occurring in clathrates of type I, (b) snub cube as found in the NaZn₁₃ structure type, (c) rhombicuboctahedron in CsNa₂Hg₁₈, (d) intermediate step between (b,c) as observed in the crystal structure of CsIn₁₂. Lower row: polyhedra for coordination number 16: (e) Frank–Kasper-type polyhedron (fourcapped truncated tetrahedron) as found in MgCu₂-type structures, (f) fourcapped hexagonal prism, realised in many AlB₂-type structures, (g) snub square antiprism in CsNa₂Hg₁₈.

An alternative visualisation of the crystal structure of CsNa₂Hg₁₈ is a net representation. This type of structure description is common for Frank–Kasper phases. The crystal structure can be subdivided into perfectly flat nets perpendicular to the tetragonal *c*-axis of the unit cell. To construct the whole crystal structure, five nets are necessary (see Figure 1, left). At height $z = 0$, a square planar net from Cs atoms on (0,0,0) is located, followed on both sides by net type B, yielding a 4.8.8 pattern of squares and octagons of Hg(1) atoms at height $z \approx 0.07$. Two of these nets form a Cs-centered octagonal prism and a set of empty [Hg₈] cubes. Net type C is located at height $z \approx 0.17$ and consists of only Hg(2) atoms,

forming a net of large and small squares with rectangles between them. The small squares augment the Cs-centered octagonal prisms to rhombicuboctahedra, while the large squares form the bases of the $[\text{NaHg}_{16}]$ snub square antiprisms. Net type D consists only of Na(1) atoms forming a square net at height $z \approx 0.20$. Net type E consists of Hg(2) and Hg(3) atoms in a square arrangement at height $z = 1/4$. Stacking of the five simple net types (taking rotations and inversions into account) is realised in a complex periodicity given in Figure 1.

Emphasising the covalent nature of the Hg sublattice would lead to a structural description of the analogy of other 3D networks, such as clathrates, zeolites or MOFs. The 3D network topology of the Hg atoms only can be analysed with, e.g., the software package ToposPro [56]. The connection pattern of the Hg network in $\text{CsNa}_2\text{Hg}_{18}$ yields a new 3D network topology with point symbol $\{3^2.4^7.5^6\}4\{3^5.4^8.5^8\}4\{3^8.4^{12}.5^8\}$.

Table 3. Standardised fractional atomic coordinates [57] and equivalent isotropic displacement parameters (\AA^2) for $\text{CsNa}_2\text{Hg}_{18}$ as a result of single-crystal structure refinement. The equivalent isotropic displacement parameter is defined as 1/3 of the trace of the anisotropic displacement tensor. All standard deviations are given in parentheses in units of the last digit.

Atom	Wyckoff Letter	Site Symmetry	x	y	z	U_{equiv}
Cs1	2a	4/ <i>mmm</i>	0	0	0	0.0325(6)
Na1	4e	4 <i>mm</i>	0	0	0.3002(7)	0.033(3)
Hg1	16n	. <i>m</i> .	0	0.29638(11)	0.42906(3)	0.0405(3)
Hg2	16m	.. <i>m</i>	0.20003(6)	<i>x</i>	0.17161(4)	0.0380(3)
Hg3	4d	$\bar{4}m2$	0	1/2	1/4	0.0409(4)

Table 4. Coefficients of the anisotropic displacement tensor (\AA^2) for $\text{CsNa}_2\text{Hg}_{18}$. U_{ij} is defined as $U_{ij} = \exp -2\pi^2 [U_{11}(ha^*)^2 + \dots + 2U_{21}hka^*b^*]$. All standard deviations are given in parentheses in units of the last digit.

Atom	U_{11}	U_{22}	U_{33}	U_{23}	U_{13}	U_{12}
Cs1	0.0322(8)	U_{11}	0.0331(13)	0	0	0
Na1	0.030(4)	U_{11}	0.038(7)	0	0	0
Hg1	0.0365(4)	0.0479(4)	0.0370(4)	−0.0032(3)	0	0
Hg2	0.0337(3)	U_{11}	0.0465(4)	0.0047(2)	U_{23}	−0.0018(2)
Hg3	0.0397(5)	U_{11}	0.0432(7)	0	0	0

Table 5. Selected interatomic distances (and their frequencies) in $\text{CsNa}_2\text{Hg}_{18}$ in \AA . All standard deviations are given in parentheses in units of the last digit. The Hg–Hg bond labels are the same as in Figure 1.

Atom 1	Atom 2	Distance	Label	Atom 1	Atom 2	Distance	Label	
Cs1	Hg2	4.0132(9) (8x)		Hg2	Hg2	2.9226(10) (2x)	I	
	Hg1	4.1925(5) (16x)			Hg1	2.9792(8) (2x)	II	
Na1	Hg2	3.150(3) (4x)		Hg3	Hg3	3.0670(5) (2x)	VI	
	Hg2	3.304(11) (4x)			Na1	3.150(3) (1x)		
	Hg1	3.370(11) (4x)			Na1	3.304(11) (1x)		
Hg1	Hg3	3.789(4) (4x)		Hg2	Hg2	3.3079(15) (1x)		
	Hg1	2.8443(14) (1x)	V		Cs1	4.0132(9) (1x)		
	Hg1	2.9759(16) (1x)	IV		Hg3	Hg2	3.0670(5) (8x)	VI
	Hg2	2.9792(8) (2x)	II			Na1	3.789(4) (4x)	
	Hg1	3.0621(12) (2x)	III			Hg1	3.8854(9) (4x)	VII
Na1	3.370(11) (1x)							
Cs1	4.1925(5) (2x)							

2.2. Chemical Bonding in CsNa₂Hg₁₈

From DFT calculations, information on the polarity of the bonding inside amalgams in the sense of high Coulombic contributions to the metallic bonding cannot directly be derived. However, there exist several typical indications for a disturbance of the conduction electrons by strong local electric fields caused by ionic bonding contributions. The DOS and pDOS plots are shown in Figure 4. The individual pDOS curves are multiplied, taking into account the respective site multiplicities. At the Fermi level, the density of states has a pronounced local minimum, yet it is non-zero. This is one of the characteristic features of a metal with a relatively low charge carrier concentration. The partial densities of states for the alkali metals is also non-zero, however, with a pronounced minimum at the Fermi level. This can be interpreted as partial electron transfer, resulting in partially positively charged atoms in the sense of Cs^{δ+}(Na^{δ+})₂[Hg₁₈]^{δ-}. As the local minima in the pDOS of Na and Cs are not very pronounced, one can assume δ, the overall polarity, to not be very large. The respective partial negative charge is distributed rather evenly over all atomic sites of the Hg lattice, according to the calculated Bader charges (see Table 6). The differences in charge distribution (Hg3 has a slightly lower partial charge than Hg1 and Hg2) may be the result of longer Hg3–Na contacts (see Table 5). The electron density on the bond critical points is very low for the Hg–Na and Hg–Cs contacts and significantly higher for the Hg–Hg contacts, indicating ionic Hg–alkali metal and covalent Hg–Hg interactions. The rather uniform electron density distribution amongst Hg atoms can be seen not only in the Bader charges but also in the very similar pDOS curves in the region around E_F for all three crystallographically different Hg sites. Another typical feature in the DOS curves of Hg-rich amalgams with high polarity is the broad range of energy over which *d*, *s* and *p*-states are spread. This mixing is common for systems with predominantly covalent Hg–Hg interactions.

Table 6. Details of the calculation of the electronic structure of Cs₂NaHg₁₈ together with Bader charges and bond critical points. The Hg–Hg bond labels are the same as in Figure 1.

Calculation details			
R _{mt} (all atoms)			132.3 pm (2.5 a.u.)
R _{mt} · K _{max}			8.0
k-points/BZ			1000
k-points/IBZ			99
Monkhorst-Pack grid			10 × 10 × 10
Bader charges			
	Na	+0.819	
	Cs	+0.763	
	Hg1	−0.113	
	Hg2	−0.169	
	Hg3	−0.074	
Bond critical points			
ρ _{B_{CP}} (e [−] Å ^{−3})	Bond	dist. (Å)	label
0.0312	Cs–Hg1	4.1925(5)	
0.0395	Cs–Hg2	4.0132(9)	
0.0581	Na–Hg2	3.150(3)	
0.0488	Na–Hg2	3.304(11)	
0.3041	Hg1–Hg1	2.8443(14)	V
0.2414	Hg1–Hg1	2.9759(16)	IV
0.2429	Hg1–Hg2	2.9792(8)	II
0.2081	Hg1–Hg1	3.0621(12)	III
0.2670	Hg2–Hg2	2.9226(10)	I
0.2061	Hg2–Hg3	3.0670(5)	VI

The specific resistivity of $\text{CsNa}_2\text{Hg}_{18}$ is shown in Figure 5 and reflects the macroscopic aspects of the electronic situation. The ‘bad metal behaviour’ [58], consisting of high specific resistivity with steep temperature dependence, is present. However, a typical deviation from the linear temperature dependence and a low Ioffe–Regel limit [59] cannot be discerned up to room temperature. For comparison, the specific resistivities of elemental Hg and the amalgam KHg_6 [44] with an equal A:Hg ratio are shown. From the band structure calculations, a relatively small polarity was seen, and the lower extent of ‘bad metal behaviour’ visible in the specific resistivity plot corroborates this finding. From direct comparisons, it can be assumed that parameters additional to the Hg content of an amalgam contribute to the macroscopic physical behaviour, such as phononic contributions, structural complexity or defects.

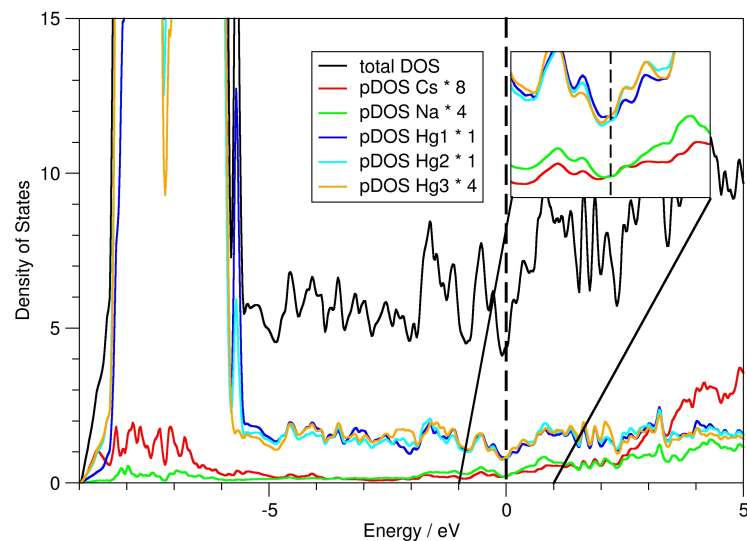


Figure 4. Density of states (DOS) and partial density of states (pDOS) curves for $\text{CsNa}_2\text{Hg}_{18}$ and the individual atomic sites therein. The Fermi energy is marked as a dashed vertical line. The region ± 1 eV around the Fermi energy is magnified in the inset.

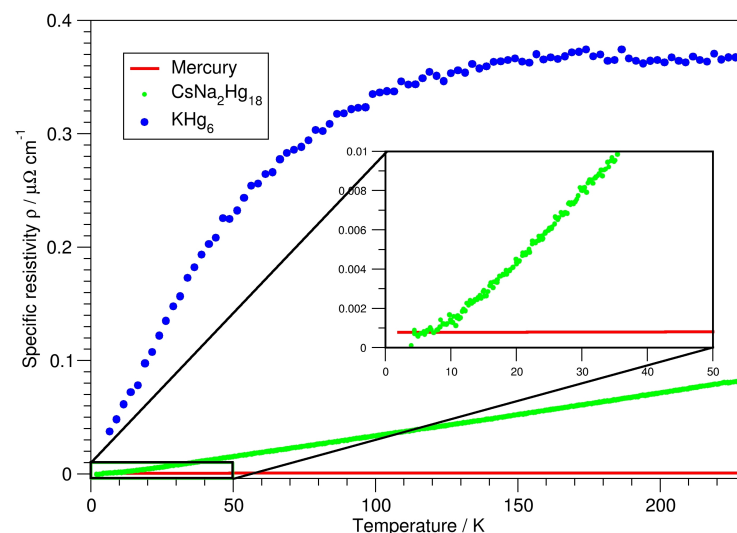


Figure 5. Specific resistivity of $\text{CsNa}_2\text{Hg}_{18}$ (green) versus temperature, in comparison to the specific resistivities of pure mercury (red) and KHg_6 (blue).

3. Materials and Methods

3.1. Synthesis

Due to the high sensitivity of the alkali metals and also the reaction products, all experiments were carried out under inert gas conditions, either inside an argon-filled glove box ($p(\text{H}_2\text{O})$ and $p(\text{O}_2) < 0.1$ ppm) or with the use of a Schlenk apparatus (vacuum/argon). Prior to the preparation of the amalgams, mercury was cleaned by filtration, subsequent stirring in half-concentrated HNO_3 to dissolve incorporated less noble metallic impurities and organic adhesions, and then distilled twice in vacuum. For the synthesis of $\text{CsNa}_2\text{Hg}_{18}$, metallic sodium (distilled twice, MPI FKF Stuttgart, Germany) and cesium (donated by Kriminalpolizei Heilbronn, Germany) were mixed with elemental mercury and heated in glass tubes. First, single crystals were taken from a sample containing 975.0 mg (7.3 mmol) Cs, 162.0 mg (7.0 mmol) Na and 11.79 g (58.8 mmol) Hg, which were mixed under ice cooling in a Schlenk tube. The reaction of the alkali metals with elemental Hg is very exothermic. The mixture was heated with a hot air gun to 300 °C until a homogeneous melt was obtained and cooled slowly to room temperature. The mass was crushed, and a powder diffraction pattern showed the presence of $\text{Cs}_3\text{Hg}_{20}$ together with NaHg_2 as only impurities. This powder was subsequently mixed with an additional 5 g (49.9 mmol) of Hg and the mixture was tempered at 105 °C for 5 months. Afterwards, surplus Hg was filtered off with a frit under an argon atmosphere. The solid contained well-crystallised cuboid specimens of $\text{CsNa}_2\text{Hg}_{18}$.

In a second synthesis attempt, a stoichiometric mixture of the elements, heated to 300 °C, quenched on ice and tempered at 105 °C for 2 weeks, yielded $\text{CsNa}_2\text{Hg}_{18}$ as the main phase, containing 6.3 at.-% of $\text{Cs}_3\text{Hg}_{20}$.

In an optimised synthesis, 217.3 mg (9.45 mmol) Na and 624.4 mg (4.70 mmol) Cs were mixed in a Schlenk tube and cooled to -78 °C with a dry ice cooling bath. The stoichiometric amount of 17.071 g (85.1 mmol) Hg was added slowly and dropwise. The mixture was allowed to thaw together with the cooling bath to room temperature overnight. The resulting product showed no impurity lines in the powder diagrams. After synthesis, the sample containers were transferred to a glove box, and small portions of the air- and moisture-sensitive samples were brought to air under potassium-dried paraffin oil for optical inspection and crystal preparation for diffraction experiments.

3.2. Powder Diffractometry

For powder diffractometry, representative parts of the product of an optimised synthesis were ground in an agate mortar inside an argon-filled glove box. In order to obtain fine powder from the slightly ductile sample, diamond powder (Sigma Aldrich, synthetic monocrystalline powder, <1 μm , dried by heating in vacuum) was added in an approximate volume ratio of amalgam:diamond = 1:20. The powder then was melt-sealed in thin-walled glass capillaries (Spezialglas No. 10, Hilgenberg, Malsfeld, Germany, $\varnothing = 0.5$ mm) and mounted and centred on the goniometer of a Stadi P diffractometer system (Stoe & Cie, Darmstadt, Germany, equipped with $\text{Mo-K}\alpha 1$ radiation, curved Ge monochromator and a MYTHEN 2K strip detector, Dectris, Baden-Dättwil, Switzerland). Data collection was performed in parafocusing Debye–Scherrer geometry. Multiple ranges were collected successively and added afterwards in order to optimise the signal-to-noise ratio. The powder diffraction pattern was used for a Rietveld refinement; see Figure 6 and Table 7. The refinement was performed with the program package Topas [60], taking the single crystal structure model as the starting value. The background was modeled by a shifted Chebyshev function with 20 parameters; the profiles were modeled based on instrument and sample parameters (fundamental parameter approach).

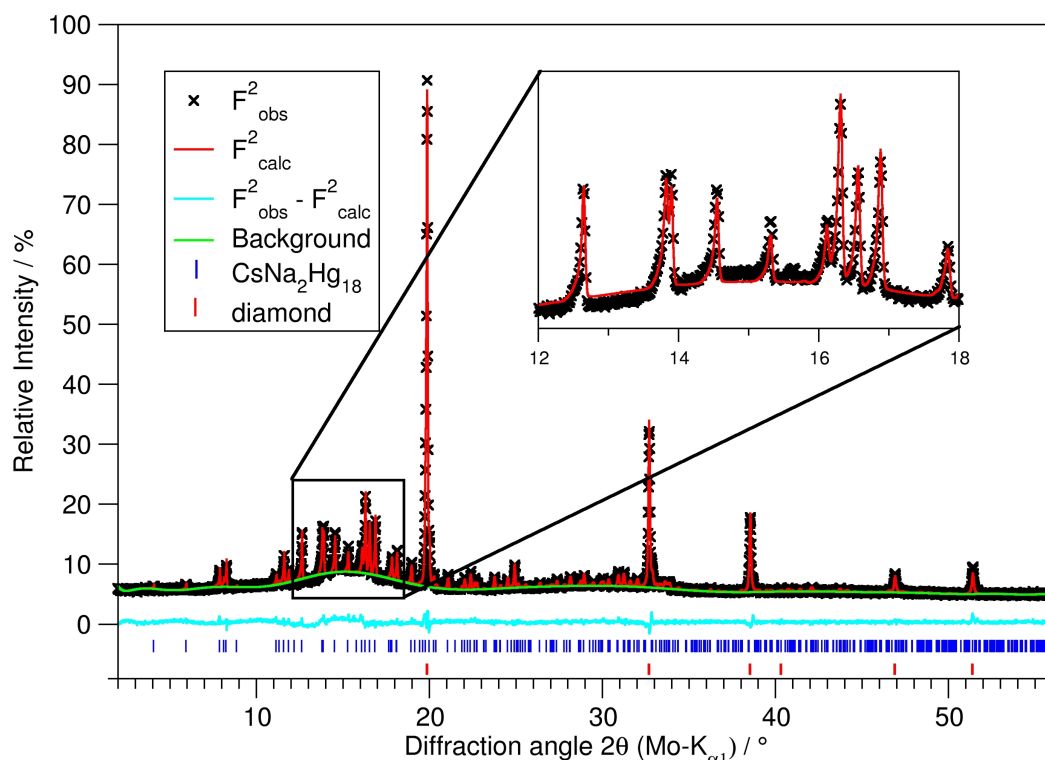


Figure 6. Rietveld refinement on a sample of phase-pure $\text{CsNa}_2\text{Hg}_{18}$, diluted with diamond powder. For details on the refinement, see Table 7.

Table 7. Crystallographic data and details on a Rietveld refinement of a phase-pure sample of $\text{CsNa}_2\text{Hg}_{18}$ as a result of an optimised synthesis. For a graphical representation of the refinement, see Figure 6. Refinement was performed with the Topas suite [60]. Below: refined fractional coordinates. In order to reach full convergence, all atoms were refined with identical values for B_{eq} of $2.39(9) \text{ pm}^2$. Standard deviations are given in units of the last digits in parentheses.

Crystal system	tetragonal
Space group	$I4/mmm$, No. 139
Lattice parameters a, c (Å)	7.3169(3), 20.058(1)
V (Å ³)	1073.9(1)
Z	2
Calc. density ($\text{g}\cdot\text{cm}^{-3}$)	11.719(1)
Radiation/wavelength (Å)	Mo- $K\alpha_1$, 0.70932
Step size (°)	0.015
Data points	3600
Diffractometer	STOE Stadi P
Detector	Dectris MYTHEN 2K
Sample geometry	capillary ($\varnothing = 0.5 \text{ mm}$)
θ range (°)	1.0–28.0
Refined parameters	35
Background function	shifted Chebyshev
Background parameters	20
Peak shape function	fundamental parameter approach
R_p / %	1.521
R_{wp} / %	2.020
R_{F^2} / %	1.220
R_{Bragg} / %	1.557
Goof on χ^2	1.656

Table 7. Cont.

Atom	x	y	z
Cs1	0	0	0
Na1	0	0	0.309(3)
Hg1	0	0.2956(5)	0.4291(2)
Hg2	0.1987(3)	x	0.1720(2)
Hg3	0	1/2	1/4

3.3. Single Crystal Diffractometry

Crystals of $\text{CsNa}_2\text{Hg}_{18}$ were found as cuboids with a metallic luster. Suitable specimens were selected under a binocular and sealed in glass capillaries ($\varnothing = 0.2$ mm) filled with paraffin oil dried over potassium sand prior to use. The capillaries were mounted and centred on the one-circle goniometer of an IPDS1 diffractometer system (Stoe & Cie, Darmstadt, Germany, Ag- $K\alpha$ radiation) in a general orientation. This was checked by evaluating the orientation matrix obtained from the indexing of 25 typically orientation frames and eventually twisting the crystal orientation with the angular slides of the goniometer head. Data collection in φ mode was performed for the accessible part of at least one-half of the Ewald sphere ($\varphi_{max} = 200^\circ$). After data collection and Lorentz and polarisation correction, the crystal shape was measured, and the faces indexed. The shape was optimised on the basis of the intensity distribution [46], and a numerical absorption correction was performed on this basis [47]. The result was compared to absorption corrections performed by other algorithms (semi-empirical on the basis of multiple recorded reflections or numerical on the basis of uncorrected crystal faces [61,62]). The high absorption coefficients, even in Ag- $K\alpha$ radiation, affords meticulous checks on data collection parameters as well as the outcome of the absorption correction processes. However, data quality is often hampered, as becomes visible from the unusual ratio of $R1$ and $wR2$ or high values for R_{int} and R_{σ} , see Table 2. This is often the case when dealing with sensitive amalgam crystals due to a superficial thin coating of the crystals with a film of liquid mercury. This film is either the result of decomposition or is a consequence of the synthesis from a mixture with excess Hg that cannot be separated entirely from the temperature-sensitive crystals by distillation or centrifugation. Taking this highly absorbing but diffusely diffracting liquid Hg film into account during absorption correction is only possible to a certain, sometimes unsatisfactory, degree.

3.4. DFT Calculations

Based on the crystal structure DFT calculations of the electronic structure, Bader charges [63] of the atomic positions were performed with the Wien2K package [64]. The full-potential linear augmented plane wave FP-LAPW was used, based on the exchange and correlation functional with generalised gradient approximation (GGA-PBE) [65]. Muffin-tin radii were assumed to 132.3 pm (2.5 a.u.) and the number of basis functions was calculated by the value of $R_{mt} \cdot K_{max} = 8.0$, with K_{max} as the largest k vector. Cutoff energies used were $E_{max}^{pot} = 196$ eV (potential) and $E_{max}^{wf} = 139$ eV (interstitial PW).

3.5. Measurement of the Specific Resistivity

Resistivity measurements were performed in a conventional 4-point van der Pauw geometry. Temperature-dependent measurements of the electric conductivity were realised with the aid of a Cryovac system between 3 and 280 K on a pellet pressed from $\text{CsNa}_2\text{Hg}_{18}$ powder. A Keithley 2400 SourceMeter as a current generator and a Hewlett-Packard 43420A Nanovoltmeter were utilised, applying a current of 1 mA. Measurements were made at Max-Planck-Institut für Festkörperforschung (Stuttgart, Germany).

4. Conclusions

Ternary amalgams containing two different electropositive metals can belong to three basic types: (1) They can form solid solutions $A_{1-x}B_xHg_n$ in the case that there are two isostructural binary amalgams AHg_n and BHg_n . This has been observed for $K_{1-x}Rb_xHg_{11}$ or for $Rb_{3-x}Cs_xHg_{20}$ [66]. (2) They can form ternary ordering variants of binary structure types, which has been observed with amalgams belonging to the $Gd_{14}Ag_{51}$ structure family, such as $Yb_{10.5}Sr_{0.5}Hg_{54}$ or $Ca_5Eu_9Hg_{51}$ [66]. (3) Finally, fully new structure types can emerge, as is shown here in the case of $CsNa_2Hg_{18}$. From the current state of our systematic studies on ternary amalgams, we see that this is by far the rarest of the three cases. All ternary amalgams show typical structural features and physical properties of polar intermetallic phases, as are already found for the binary amalgams. Enlarging the number of individual amalgam phases by transitioning from binary to ternary amalgams allows for comparative studies and for the identification of common parameters influencing the extent of ‘bad metal behaviour’. In the future, this knowledge may be transferred from the model system of amalgams to further polar intermetallics in order to deliberately tailor physical properties crucial for thermoelectric, catalytic, electronic or magnetic applications.

Author Contributions: C.H. conceptualised the studies and wrote the manuscript, T.H. performed the practical work, prepared the single crystal samples and performed all analyses, F.T. performed the DFT calculations. All authors have read and agreed to the published version of the manuscript.

Funding: This research was funded by Deutsche Forschungsgesellschaft with grant number 429690805.

Data Availability Statement: The data presented in this study are available on request from the corresponding author.

Acknowledgments: We thank Reinhard Kremer (MPI Festkörperforschung Stuttgart) for the measurements of the specific electric resistivity.

Conflicts of Interest: The authors declare no conflict of interest.

References

1. Deiseroth, H.J. Discrete and extended metal clusters in alloys with mercury and other group 12 elements. In *Molecular Clusters of the Main Group Elements*; Driess, M., Nöth, H., Eds.; Wiley-VCH: Weinheim, Germany, 2004; pp. 169–187.
2. Wendorff, M.; Röhr, C. Alkaline-earth tri-mercurides $A^{II}Hg_3$ ($A^{II} = Ca, Sr, Ba$): Binary intermetallic compounds with a common and a new structure type. *Z. Kristallogr.* **2018**, *223*, 515–529. [[CrossRef](#)]
3. Simons, J.H.; Seward, R.P. Slow electron scattering and the apparent electron affinity of mercury. *J. Chem. Phys.* **1938**, *6*, 790–794. [[CrossRef](#)]
4. Biehl, E.; Deiseroth, H.J. Crystal structure of potassiumamalgam, KHg . *Z. Kristallogr.* **1996**, *630*, 211. [[CrossRef](#)]
5. Deiseroth, H.J.; Strunck, A.; Bauhofer, W. $CsHg$, eine ungewöhnliche Variante der $CsCl$ -Struktur. Darstellung, Kristallstruktur und physikalische Eigenschaften. *Z. Anorg. Allg. Chem.* **1989**, *575*, 31–38. [[CrossRef](#)]
6. Tkachuk, A.V.; Mar, A. Redetermination of Na_3Hg_2 . *Acta Crystallogr.* **2006**, *E62*, i129–i130. [[CrossRef](#)]
7. Deiseroth, H.J.; Strunck, A. Hg_8 (Mercubane) Clusters in $Rb_{15}Hg_{16}$. *Angew. Chem. Int. Ed.* **1989**, *28*, 1251–1252. [[CrossRef](#)]
8. Deiseroth, H.J.; Stupperich, A.; Pankaluoto, R.; Christensen, N.E. $NaHg$: A variant of the cesiumchloride structure structural relations and electronic structure. *Z. Anorg. Allg. Chem.* **1991**, *597*, 41–50. [[CrossRef](#)]
9. Lihl, F. Über den Aufbau des Systems Quecksilber-Mangan. *Monatsh. Chem.* **1955**, *86*, 186–191. [[CrossRef](#)]
10. Slater, J.C. Atomic radii in crystals. *J. Chem. Phys.* **1964**, *41*, 3199–3204. [[CrossRef](#)]
11. Hoch, C.; Simon, A. $Na_{11}Hg_{52}$: Complexity in a polar metal. *Angew. Chem. Int. Ed.* **2012**, *51*, 3262–3265. [[CrossRef](#)]
12. Tambornino, F.; Sappl, J.; Hoch, C. The $Gd_{14}Ag_{51}$ structure type and its relation to some complex amalgam structures. *J. Alloys Compd.* **2015**, *618*, 326–335. [[CrossRef](#)]
13. Deiseroth, H.J.; Biehl, E. $NaK_{29}Hg_{48}$: A contradiction to or an extension of theoretical concepts to rationalize the structures of complex intermetallics. *J. Solid State Chem.* **1999**, *147*, 177–184. [[CrossRef](#)]
14. Pauly, H.; Weiss, A.; Witte, H. Kubisch flächenzentrierte Legierungen der Zusammensetzung Li_2MgX mit raumzentrierter Unterstruktur. *Z. Metallkd.* **1968**, *59*, 414–418.
15. Tkachuk, A.V.; Mar, A. $Li_6A_{17}Hg_9$ ($A = Ca, Sr, Yb$): Intermetallic compounds of mercury with a zeolite-like topology of cubic networks. *Chem. Eur. J.* **2009**, *15*, 10348–10351. [[CrossRef](#)]
16. Villars, P.; Cenzual, K. *Pearson’s Crystal Data—Crystal Structure Database for Inorganic Compounds*; ASM International: Materials Park, OH, USA, 2017.
17. Vogel, R.; Schuster, H.U. $KHgAs$ (Sb) und $KZnAs$ —Ternäre Verbindungen mit modifizierter Ni_2In -Struktur. *Z. Naturforsch.* **1980**, *B 35*, 114–116. [[CrossRef](#)]

18. Schuster, H.U. Ternäre Lithiumverbindungen vom Typ Li_2MeGe (Me = Zn, Cd, Hg). *Z. Anorg. Allg. Chem.* **1969**, *370*, 149–159. [[CrossRef](#)]
19. Lagrange, P.; Makrini, M.E.; Hérold, A. Structure cristalline du mercurographite KHgC_4 . *Rev. Chim. Minér.* **1983**, *20*, 229–246.
20. Kaltzoglou, A.; Ponou, S.; Fässler, T.F. A_4Ge_9 (A = K, Rb) as precursors for Hg-substituted clathrate-I synthesis: Crystal structure of $\text{A}_8\text{Hg}_3\text{Ge}_{43}$. *Eur. J. Inorg. Chem.* **2008**, *2008*, 4507–4510. [[CrossRef](#)]
21. Pauly, H.; Weiss, A.; Witte, H. Phasenbreite und Valenzelektronenkonzentration (VEK) in den ternären kubischen Zintlphasen vom NaTl-Typ. *Z. Metallkd.* **1968**, *59*, 554–558.
22. Kaltzoglou, A.; Ponou, S.; Fässler, T.F. Synthesis and crystal structure of mercury-substituted type-I clathrates $\text{A}_8\text{Hg}_4\text{Sn}_{42}$ (A = K, Rb, Cs). *Eur. J. Inorg. Chem.* **2008**, *2008*, 538–542. [[CrossRef](#)]
23. Matthes, R.; Schuster, H.U. Ternäre Natriumphasen mit Cadmium bzw. Quecksilber und Zinn bzw. Blei. *Z. Naturforsch.* **1980**, *B 35*, 778–780. [[CrossRef](#)]
24. Sevov, S.C.; Ostenon, J.E.; Corbett, J.D. $\text{K}_8\text{In}_{10}\text{Hg}$: A Zintl phase with isolated In_{10}Hg clusters. *J. Alloys Compd.* **1993**, *202*, 289–294. [[CrossRef](#)]
25. Ponou, S.; Kim, S.J.; Fässler, T.F. Synthesis and characterization of $\text{Na}_5\text{M}_{2+x}\text{Sn}_{10-x}$ ($x \approx 0.5$, M = Zn, Hg) - A doped tetrahedral framework structure. *J. Am. Chem. Soc.* **2009**, *131*, 10246–10252. [[CrossRef](#)] [[PubMed](#)]
26. Schmidt, P.C.; Baden, W.; Weiden, N.; Weiss, A. The Intermetallic System $\text{NaHg}_{1-x}\text{Tl}_x$. X-ray Investigations and Measurements of the Knight Shift of Na, Hg, and Tl. *Phys. Status Solidi* **1985**, *A92*, 205–212. [[CrossRef](#)]
27. Fox, J.M.; Henry, P.F.; Rosseinsky, M.J. $\text{Na}_{2+x}\text{Hg}_y\text{C}_{60}$: Post-transition metal intercalation chemistry of a C_{60} host. *Chem. Commun.* **1996**, *1996*, 2299–2300. [[CrossRef](#)]
28. Wendorff, M.; Röhr, C. Barium-Triel-Mercuride $\text{BaM}_x\text{Hg}_{4-x}$ und $\text{Ba}_3\text{M}_x\text{Hg}_{11-x}$ (M = Ga, In, Cd). *Z. Naturforsch.* **2013**, *B68*, 307–322. [[CrossRef](#)]
29. Zheng, L.; Feng, Y.; Wang, R.; Chen, Y. Crystal structure and properties of the new ternary compound $\text{Mg}_{21}\text{Ga}_5\text{Hg}_3$. *Intermetallics* **2009**, *17*, 873–877. [[CrossRef](#)]
30. Daams, J.L.C.; Vucht, J.H.N.V. Contribution to the system Mg-Au-Hg. *Philips J. Res.* **1984**, *39*, 275–292.
31. Dai, J.C.; Corbett, J.D. Substitution of Au or Hg into BaTl_2 and BaIn_2 . New ternary examples of smaller CeCu_2 -type intermetallic phases. *Inorg. Chem.* **2006**, *45*, 2104–2111. [[CrossRef](#)]
32. Wendorff, M.; Schwarz, M.R.; Röhr, C. The new Hg-rich barium indium mercurides $\text{BaIn}_x\text{Hg}_{7-x}$ ($x = 3.1$) and $\text{BaIn}_x\text{Hg}_{11-x}$ ($x = 0-2.8$). Synthesis, crystal and electronic structure. *J. Solid State Chem.* **2013**, *203*, 297–303. [[CrossRef](#)]
33. Merlo, F.; Pani, M.; Fornasini, M.L. RMX compounds formed by alkaline earths, europium and ytterbium. III. Ternary phases with M = Mg, Hg and X = Si, Ge, Sn, Pb. *J. Alloys Compd.* **1993**, *196*, 145–148. [[CrossRef](#)]
34. Wendorff, M.; Röhr, C. The new barium mercuride BaHg_6 and ternary indium and gallium derivatives. *J. Alloys Compd.* **2013**, *546*, 320–328. [[CrossRef](#)]
35. Puseelj, M.; Ban, Z. Ternäre Gamma-Messing Phasen in den Systemen Calcium-M(Ib/IIb)-Quecksilber. *Z. Naturforsch.* **1980**, *B35*, 1594–1595. [[CrossRef](#)]
36. Dai, J.C.; Gupta, S.; Gourdon, O.; Kim, H.J.; Corbett, J.D. BaHg_2Tl_2 . An unusual polar intermetallic phase with strong differentiation between the neighboring elements mercury and thallium. *J. Am. Chem. Soc.* **2009**, *131*, 8677–8682. [[CrossRef](#)]
37. Dai, J.C.; Gupta, S.; Corbett, J.D. Synthesis, structure, and bonding of BaTl_4 . Size effects on encapsulation of cations in electron-poor metal networks. *Inorg. Chem.* **2011**, *50*, 238–244. [[CrossRef](#)]
38. Melnychenko, N.O. Solid solution based clathrate $\text{Ba}_8\text{Ge}_{43}(\text{O})_3$ (O = vacancy) with transition elements. *Nauk. Visn. Uzhhorod. Univ. Ser. Khim.* **2013**, *30*, 46–49.
39. Schwarz, M.R.; Wendorff, M.; Röhr, C. The new barium zinc mercurides $\text{Ba}_3\text{ZnHg}_{10}$ and $\text{BaZn}_{0.6}\text{Hg}_{3.4}$ —Synthesis, crystal and electronic structure. *J. Solid State Chem.* **2012**, *196*, 416–424. [[CrossRef](#)]
40. Wendorff, M.; Röhr, C. Strontium metallides along the section $\text{SrIn}_4\text{-SrHg}_4$. *Z. Naturforsch.* **2014**, *B69*, 388–408. [[CrossRef](#)]
41. Wendorff, M.; Röhr, C. The new complex barium mercuride $\text{Ba}_{20}\text{Hg}_{103}$ and its ternary zinc and cadmium variants. *Z. Naturforsch.* **2012**, *B67*, 893–906. [[CrossRef](#)]
42. Iandelli, A. The structure of some ternary intermetallic compounds of the rare earths. *J. Alloys Compd.* **1994**, *203*, 137–138. [[CrossRef](#)]
43. Weitzer, F.; Leithe-Jasper, A.; Rogl, P.; Hiebl, K.; Rainbacher, A.; Wiesinger, G.; Steiner, W.; Friedl, J.; Wagner, F.E. Magnetism of ternary compounds $\text{RE}_6\text{Fe}_{13}\text{X}$; RE = Pr, Nd; X = Cu, Ag, Au, Zn, Cd, and Hg. *J. Appl. Phys.* **1994**, *75*, 7745–7751. [[CrossRef](#)]
44. Tambornino, F.; Hoch, C. Bad metal behaviour in the new Hg-rich amalgam KHg_6 with polar metallic bonding. *J. Alloys Compd.* **2015**, *618*, 299–304. [[CrossRef](#)]
45. Tambornino, F.; Schwärzer, K.; Hoch, C. Synthesis and characterization of $\text{La}_{11+x}\text{Hg}_{45-x}$ and $\text{RE}_{11}\text{Hg}_{45.5}$ (RE = Sm, Nd) as hettotypes of the $\text{Sm}_{11}\text{Cd}_{45}$ structure type. *J. Solid State Chem.* **2016**, *242*, 162–169. [[CrossRef](#)]
46. Stoe & Cie. X-SHAPE v. 2.07; Stoe & Cie: Darmstadt, Germany, 2005.
47. Stoe & Cie. X-RED v. 1.31; Stoe & Cie: Darmstadt, Germany, 2005.
48. Sheldrick, G.M. A short history of SHELX. *Acta Crystallogr.* **2008**, *A64*, 112–122. [[CrossRef](#)] [[PubMed](#)]
49. Tambornino, F.; Sappl, J.; Pultar, F.; Cong, T.M.; Hübner, S.; Giffthaler, T.; Hoch, C. Electrocrystallization—A synthetic method for intermetallic phases with polar metal-metal bonding. *Inorg. Chem.* **2016**, *55*, 11551–11559. [[CrossRef](#)]

50. Deiseroth, H.J.; Toelstede, D. Na₃Hg: Das natriumreichste Amalgam im System Natrium-Quecksilber. *Z. Anorg. Allg. Chem.* **1992**, *615*, 43–48. [[CrossRef](#)]
51. Deiseroth, H.J.; Toelstede, D. Na₈Hg₃: Ein alkalimetallreiches Amalgam mit isolierten Quecksilberanionen? *Z. Anorg. Allg. Chem.* **1990**, *587*, 103–109. [[CrossRef](#)]
52. Nielsen, J.W.; Baenziger, N.C. The crystal structures of NaHg₂, NaHg and Na₃Hg₂. *Acta Crystallogr.* **1954**, *7*, 277–282. [[CrossRef](#)]
53. Deiseroth, H.J.; Strunck, A.; Bauhofer, W. RbHg₂ und CsHg₂, Darstellung, Kristallstruktur, elektrische Leitfähigkeit. *Z. Anorg. Allg. Chem.* **1988**, *558*, 128–136. [[CrossRef](#)]
54. Todorov, E.; Sevov, S.C. Synthesis and structure of the alkali metal amalgams A₃Hg₂₀ (A = Rb, Cs), K₃Hg₁₁, Cs₅Hg₁₉, and A₇Hg₃₁ (A = K, Rb). *J. Solid State Chem.* **2000**, *149*, 419–427. [[CrossRef](#)]
55. Hoch, C.; Simon, A. Cs₂Hg₂₇, the mercury-richest amalgam with close relationship to the Bergman phases. *Z. Anorg. Allg. Chem.* **2008**, *634*, 853–856. [[CrossRef](#)]
56. Blatov, V.A.; Shevchenko, A.P.; Proserpio, D.M. Applied topological analysis of crystal structures with the program package ToposPro. *Cryst. Growth Des.* **2014**, *14*, 3576–3586. [[CrossRef](#)]
57. Gelato, L.M.; Parthé, E. Structure Tidy—A computer program to standardize crystal structure data. *J. Appl. Cryst.* **1987**, *20*, 139–143. [[CrossRef](#)]
58. Gunnarsson, O.; Calandra, M.; Han, J.E. Saturation of electrical resistivity. *Rev. Mod. Phys.* **2003**, *75*, 1085. [[CrossRef](#)]
59. Ioffe, A.F.; Regel, A.R. Non-crystalline, amorphous and liquid electronic semiconductors. *Prog. Semicond.* **1960**, *4*, 237–291.
60. Coelho, A.A. TOPAS and TOPAS-Academic: An optimization program integrating computer algebra and crystallographic objects written in C++. *J. Appl. Cryst.* **2018**, *51*, 210–218. [[CrossRef](#)]
61. Spek, A.L. Single-crystal structure validation with the program PLATON. *J. Appl. Cryst.* **2002**, *36*, 7–13. [[CrossRef](#)]
62. Alcock, N.W. Crystal measurements for absorption correction. *Acta Crystallogr.* **1970**, *A26*, 437–439. [[CrossRef](#)]
63. Bader, R.F.W. A quantum theory of molecular structure and its applications. *Chem. Rev.* **1991**, *91*, 893–928. [[CrossRef](#)]
64. Blaha, P.; Schwarz, K.; Tran, F.; Laskowski, R.; Madsen, G.K.H.; Marks, L.D. WIEN2k: An APW-*lo* program for calculating the properties of solids. *J. Chem. Phys.* **2020**, *152*, 074101. [[CrossRef](#)]
65. Perdew, J.P.; Burke, K.; Ernzerhof, M. Generalized gradient approximation made simple. *Phys. Rev. Lett.* **1996**, *77*, 3865. [[CrossRef](#)] [[PubMed](#)]
66. Hohl, T.; Kremer, R.; Ebbinghaus, S.; Hoch, C. Influence of disorder on the ‘bad metal behaviour’ in polar amalgams. Manuscript in preparation.